Formation of the Inhibitory Complex of *p*-Mercuribenzoate with Xanthine Oxidase, Evaluation of Hyperfine and Quadrupole Couplings of Mercury to Molybdenum(V) from the Electron Paramagnetic Resonance Spectrum, and Structure of the Complex†

Graham N. George and Robert C. Bray*

ABSTRACT: The reaction of *p*-mercuribenzoate with the molybdenum center of xanthine oxidase has been investigated. Kinetic analysis showed that the mechanism involves relatively slow but reversible binding of the inhibitor to the enzyme, which reacts when in the reduced state only. The rate constant for formation of the inhibitory complex at pH 8.2 and 23.5 °C is about 10^4 M^{-1} s^{-1}, and its dissociation constant is about 3 μM. Since the inhibitory reaction is shown to be associated with the appearance of a new Mo(V) electron paramagnetic resonance (EPR) signal (the Mercurial signal), this reaction must take place at the molybdenum center. No comparable reaction takes place with desulfo xanthine oxidase. The Mercurial signal disappears and enzymic activity returns on exposing the enzyme to oxygen. Similar kinetic and EPR results were obtained with a number of related mercurial compounds. The Mercurial signal has been investigated in detail with the help of *p*-mercuribenzoate enriched with ^{199}Hg ($I = {}^1/_2$) and with ^{201}Hg ($I = {}^3/_2$). Spectra from the various isotopes recorded at 9 and at 35 GHz were accurately simulated when a single set of parameters was used. *g* values are 1.9434, 1.9581, and 1.9687. There is strong hyperfine coupling of ^{199}Hg to Mo(V) with **A**(^{199}Hg) = 272, 285, and 443 MHz; angles between the **g** and **A** axes have been determined but are small. For ^{201}Hg, the spectrum is dominated by strong nuclear quadrupole coupling of 960 MHz. Additional information has been obtained by measuring couplings of Mo(V) in the signal to ^{33}S (A_{av} = 10.0 MHz) and to ^{17}O (A_{av} = 15.4 MHz) in the enzyme. It is concluded that the inhibitory complex has the structure Mo–S–Hg–, which is analogous to that in the arsenite complex of the enzyme [George, G. N., & Bray, R. C. (1983) *Biochemistry 22*, 1013–1021]. The directions of the strongest hyperfine and quadrupole couplings coincide and probably lie along the linear sp bonding system of mercury. Overall, the data further confirm the presence [Gutteridge, S., Tanner, S. J., & Bray, R. C. (1978) *Biochem. J. 175*, 887–897] of a catalytically important Mo–S–H group in reduced xanthine oxidase.

For many years, *p*-mercuribenzoate has been used as an inhibitor of enzymes containing essential thiol groups in their active centers. It was first shown to inhibit xanthine oxidase by Harris & Hellerman (1956), and shortly afterwards, Fridovich & Handler (1958) reported that substrates potentiated the action of the compound on the enzyme. This work was extended somewhat by Brumby et al. (1965) and by Massey et al. (1969) and seems to indicate that a thiol is present in reduced xanthine oxiddase that is unavailable in the oxidized enzyme. However, from a kinetic viewpoint, the inhibition has never been fully characterized.

According to the latest information [see Bray & Gutteridge (1982) for references], the action of xanthine oxidase on substrates involves abstraction of a substrate proton by the enzyme, the acceptor group being Mo=S, which is converted in this process to Mo–SH (Gutteridge et al., 1978a,b). The possibility therefore immediately arises that this molybdenum-bound thiol is the one that reacts with *p*-mercuribenzoate. If this were the case, then large changes in the EPR[1] spectrum of molybdenum(V) in the enzyme might be expected to accompany reaction of the mercurial, since the proton in the acceptor site is known to be strongly coupled to molybdenum (Gutteridge et al., 1978a).

EPR spectroscopy of molybdenum(V) has indeed been revealing in studies of the structure and action of the molybdenum center of xanthine oxidase (Bray, 1980; Bray & Gutteridge, 1982). Particularly pertinent is the conclusion (George & Bray, 1983) that arsenite,[2] earlier thought (Massey & Edmondson, 1970) to react with a thiol and a persulfide in the active center, instead reacts with the Mo–SH group. The present study was undertaken to test the hypothesis that *p*-mercuribenzoate also reacts with the Mo–SH group and has confirmed this to be the case. We have also carried out kinetic investigations, with a view to futher characterizing the inhibition. The EPR work may be of some chemical interest, in addition to its relevance to the mechanism of xanthine oxidase action. Thus, analogously to George & Bray (1983), we were able, from the molybdenum EPR spectrum, to evaluate not only **g** and **A** tensors but also the quadrupole coupling tensor for ^{201}Hg. This appears to be the first occasion on which the quadrupole coupling of mercury has been fully evaluated by simulation from a "powder-type" EPR spectrum.

Materials and Methods

Xanthine Oxidase and Chemicals. Xanthine oxidase was prepared according to Hart et al. (1970) and Bray (1982). Concentrations of the functional enzyme were calculated according to Bray (1975). Conversion to the desulfo enzyme

† From the School of Chemistry and Molecular Sciences, University of Sussex, Falmer, Brighton BN1 9QJ, England. *Received April 1, 1983.* The work was supported by grants from the Medical Research Council and the Science and Engineering Research Council; G.N.G. received a Studentship from the latter.

[1] Abbreviations: EPR, electron paramagnetic resonance; EXAFS, X-ray absorption edge extended fine structure; Bicine, *N*,*N*-bis(2-hydroxyethyl)glycine; NQR, nuclear quadrupole resonance.

[2] Since this work was completed, two further publications on the arsenite complex of xanthine oxidase have come to our attention (Hille et al., 1983; Barber & Siegel, 1983). In the latter, the Arsenite EPR signal has clearly been misinterpreted [cf. George & Bray (1983)].

0006-2960/83/0422-5443$01.50/0

was carried out according to Massey & Edmondson (1970). Isotopic-enrichment studies with ^{17}O and ^{33}S were carried out as described by George & Bray (1983). ^{95}Mo-enriched xanthine oxidase was from the work of Pick et al. (1971), stored over liquid nitrogen from that time. The following mercurial compounds were obtained from Sigma Limited: *p*-(chloromercuri)benzoic acid (*p*-mercuribenzoate), *p*-(chloromercuri)benzenesulfonic acid (*p*-mercuribenzenesulfonate), (*p*-aminophenyl)mercuric acetate (*p*-mercurianiline), and phenylmercuric acetate (phenylmercuric ions). The names in parentheses are those used in the text. Other chemicals were of normal laboratory reagent grade.

Analysis of Spectrophotometric Time-Course Data. Progress curves for conversion of xanthine to uric acid were followed at 295 nm (Hart et al., 1970) by using a Pye-Unicam SP 1800 recording spectrophotometer. The curves were digitized manually, and theoretical curves were fitted to them by using an iterative computer procedure that minimized the sum of squares error between experimental and calculated points.

Isotopically Enriched p-Mercuribenzoate. *p*-Mercuribenzoate was synthesized on a small scale (5 mg of HgO) by conversion of *p*-bromotoluene to the Grignard reagent and reaction of this with $HgCl_2$, followed by oxidation with alkaline $KMnO_4$ (Whitmore & Woodward, 1941). ^{201}Hg (92.0% enriched, containing 0.3% ^{199}Hg) and ^{199}Hg (85.3% enriched, containing 1.8% ^{201}Hg) were obtained as HgO from Oak Ridge National Laboratory, TN. They were converted to $HgCl_2$ by dissolving them in HCl and evaporating to dryness. The Grignard reagent was prepared from a 2 M solution of *p*-bromotoluene in ether (dried over sodium), which was added to an excess of magnesium powder and left for 30 min. A 0.1-mL aliquot of this Grignard reagent solution (i.e., a 2-fold excess) was added to $HgCl_2$ (from 5 mg of HgO) dissolved in 0.1 mL of dry ether. A white precipitate formed and was collected by centrifugation. To the precipitate was added 0.2 mL of 0.25 M $KMnO_4$ in 1.7 M NaOH, and the sample was heated to 95 °C for 15 min. After the addition of an excess of ethanol, the solution was centrifuged to remove precipitated MnO_2. Concentrated HCl was added until a white precipitate no longer formed. The precipitate was centrifuged off and dried and then recrystallized from 0.1 mL of hot acetone. The product obtained by this procedure was identical with commercial *p*-mercuribenzoate (Sigma) in its inhibitory action on xanthine oxidase. When prepared by a similar procedure but on a larger scale, it had a melting point of 278 °C (lit. mp 273 °C) and NMR and IR spectra identical with the commercial material and gave similar microanalysis (carbon and hydrogen).

Preparation of Samples of Xanthine Oxidase for EPR Measurements. Samples of the enzyme (usually about 0.2 mM) were reduced with dithionite under an atmosphere of purified argon and then frozen in liquid nitrogen, after the reaction times indicated, following, where appropriate, addition of the mercurial compound. Fast kinetic studies were carried out by rapid freezing according to Gutteridge et al. (1978a).

Recording and Simulation of EPR Spectra. EPR spectra were recorded on frozen samples on a Varian E9 spectrometer linked to a PDP 11/10 computer and visual display system (Bray et al., 1978). Computer simulation of EPR spectra was performed on the University of Sussex DEC VAX 11/780 computer. Simulations involving quadrupole coupling were performed by using the program QPOW of R. L. Belford and co-workers (Nilges, 1979; Belford & Nilges, 1979; Maurice, 1980), as in our earlier work (George & Bray, 1983). Other simulations used simpler programs [cf. Lowe (1978)], with provision for noncoincident axes of **A** and **g** (Malthouse et al., 1981; George 1983). In all cases, simulation was performed on-line to the computer, with software (George, 1983) that allowed display of the experimental and simulated spectra superimposed and calculation of the sum-of-squares error for the fit.

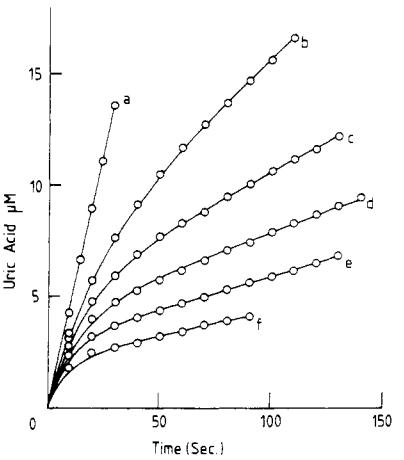

FIGURE 1: Xanthine oxidase assays in the presence of various concentrations of *p*-mercuribenzoate. Xanthine oxidase was added to enzyme assay mixtures containing various *p*-mercuribenzoate concentrations as follows: (a) control (no *p*-mercuribenzoate), (b) 5 μM, (c) 10 μM, (d) 15 μM, (e) 20 μM, and (f) 30 μM. The points are experimental values measured from spectrophotometer traces at 295 nm, and the curves are calculated by fitting to eq 1 (see the text) by using a least-squares fitting procedure. The buffer was 50 mM Na^+–Bicine, pH 8.2, the xanthine concentration was 100 μM, the enzyme concentration was ~23 nM, and the temperature was 23.5 °C.

Results and Discussion

Kinetics of Inhibition of Xanthine Oxidase by p-Mercuribenzoate or Other Mercurials. We first carried out kinetic investigations of the inhibition by *p*-mercuribenzoate by using the standard spectrophotometric xanthine oxidase assay. Earlier work (Brumby et al., 1965) indicated that the inhibition occurred by two distinct processes, a rapid and reversible process and a slower, nonreversible reaction. The latter occurred at high concentrations of the mercurial, and most readily in the presence of substrate, and was paralleled by loss of flavin, iron, and acid-labile sulfur from the enzyme. Since only the reversible reaction was of interest in the present work, we sought, whenever possible, to minimize the extent of the nonreversible reaction by working at low concentrations of the inhibitor.

In the assay of xanthine oxidase, with xanthine as a substrate, the graph of uric acid production is linear for at least 15% of the overall reaction (see Figure 1, curve a). When the assay was conducted in the presence of *p*-mercuribenzoate, a time-dependent decrease in the reaction rate was observed, which was markedly dependent upon the concentration of the inhibitor (Figure 1, curves b–g). Such slowly developing inhibition, which procedes not to complete inhibition but to an inhibited steady state, may be analyzed by procedures described by Cha (1975, 1976). Accordingly, the curves through the experimental points in Figure 1 are theoretical ones, calculated by fitting the data to eq 1 or to the integrated form

$$v = v_s + (v_0 - v_s)e^{-k_{obsd}t} \quad (1)$$

of this. In eq 1, v_s is the final (steady-state) velocity, v_0 is the observed initial velocity, and k_{obsd} is a rate constant that is characteristic of the inhibition process.

Table I: Parameters Describing Inhibition of Xanthine Oxidase by Different Mercurials[a]

mercurial	k_{obsd} (s^{-1})	v_s/v_0
p-Hg^+-C_6H_4-COO^-	0.11	0.07
p-Hg^+-C_6H_4-SO_3^-	0.10	0.07
p-Hg^+-C_6H_4-NH_3^+	0.020	0.38
p-Hg^+-C_6H_4-CH_3	0.027	0.28
p-Hg^+-C_6H_5	0.030	0.39

[a] Experiments of the type illustrated in Figure 1 were carried out at pH 8.2 and 23.5 °C in 50 mM Na^+-Bicine buffer, with the inhibitor at a concentration of 20 μM, in the presence of 100 μM xanthine. The parameters k_{obsd} and v_s/v_0 of eq 1 (see the text) were obtained from computer fitting to the progress curves [cf. Cha (1976)].

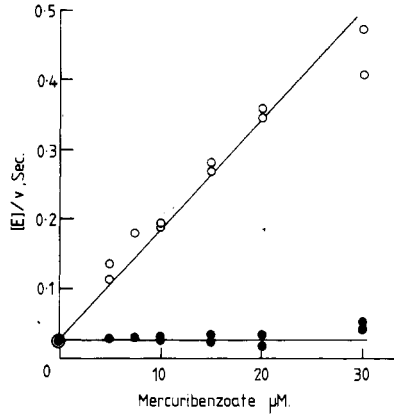

FIGURE 2: Effect of variation in p-mercuribenzoate concentration upon initial (v_0) and steady-state (v_s) velocities in xanthine oxidase assays. Plots of the inverse of initial (●) and steady-state (○) velocities vs. p-mercucribenzoate concentration are shown. The points were obtained from computer fits to experimental data such as those shown in Figure 1. Velocities are expressed as catalytic-center activities $v/[E]$.

We carried out experiments of the type illustrated in Figure 1 for a series of mercurials of general formula:

$$p\text{-}Hg^+\text{-}C_6H_4\text{-}R$$

It was considered that the nature of the group R might change the effectiveness of the mercurial in inhibiting xanthine oxidase, and this was indeed found to be the case. Results are summarized in Table I in the form of the ratio v_s/v_0 and of k_{obsd}, both obtained in the presence of the inhibitor at a concentration of 20 μM. It can be seen that p-mercuribenzoate, along with p-mercuribenzenesulfonate, is both the quickest acting and the most effective inhibitor. The data thus indicate that a negatively charged R group potentiates the effectiveness of the mercurial, presumably by interacting with a positively charged group [see, e.g., Nishino et al. (1982)] in the active site.

We carried out more detailed investigations with p-mercuribenzoate, studying, first, the effect of pH on the inhibition. Results (not illustrated) showed that k_{obsd} exhibited some dependence on the buffer and went through a minimum value at about pH 8.2 (the pH value at which most of our experiments were carried out), with inhibition developing more rapidly at both higher and lower pH values. On the other hand, v_s/v_0 increased progressively with increasing pH, between pH 6 and 10.

Results from experiments at pH 8.2, again of the type illustrated in Figure 1, and carried out at a series of different concentrations of p-mercuribenzoate are summarized in Figures 2 and 3. Before discussing these results, we have to consider the reverse process. Figure 4 shows the time course of reversal of inhibition, following dilution of xanthine oxidase

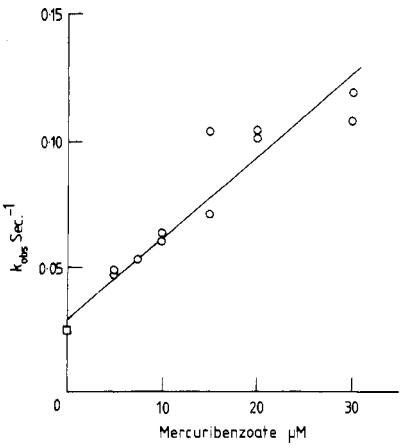

FIGURE 3: Effect of variation in p-mercuribenzoate concentration on pseudo-first-order rate constant (k_{obsd}) for conversion between initial and steady-state velocities in xanthine oxidase assays. The values for the observed rate constant (k_{obsd}) were obtained from computer fits to experiments such as those shown in Figure 1 (○). The single point (□) was from the computer fit to the experiment in Figure 4. These values are plotted against p-mercuribenzoate concentration.

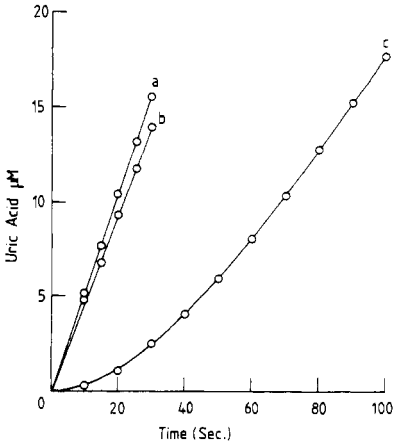

FIGURE 4: Effect upon xanthine oxidase assays of preincubating enzyme with p-mercuribenzoate. Xanthine oxidase (~0.15 mM) was preincubated anaerobically for 30 s with 1 mM xanthine (a), with 1 mM p-mercuribenzoate (b), or with 1 mM p-mercuribenzoate plus 1 mM xanthine (c). 1-μL samples were withdrawn and added to 3 mL of assay mixture (100 μM xanthine in 50 mM Na^+-Bicine, pH 8.2, at 23.5 °C), and the reaction was followed spectrophotometrically at 295 nm. For curves b and c, the final concentration of p-mercuribenzoate in the assay was thus only 0.33 μM. As in Figure 1, the points represent experimental data (measured from spectrophotometer traces), and the solid curve c represents a computer fit to eq 1 (see the text).

that had been preincubated, under conditions designed to give essentially 100% inhibition, with a relatively high concentration of p-mercuribenzoate. A time-dependent recovery of activity was observed (Figure 4, curve c), presumably due to the slow release of bound p-mercuribenzoate from the enzyme. In experiments where no reducing agent was included in the preincubation mixture (consisting of p-mercuribenzoate and xanthine oxidase only), this behavior was not observed (Figure 4, curve b). According to Cha (1976), such data may be analyzed, in the same way as was done for the experiments of Figure 1, by fitting it to eq 1. However, it is apparent that the final velocity, v_s, in curve c of Figure 4 is lower than the velocity in the control curves a and b. This is attributed to a permanent loss of activity in some molecules due to removal of Fe/S and flavin centers (Brumby et al., 1965), which would be expected at the high p-mercuribenzoate concentration used (1 mM).

Table II: Parameters for Mercurial and for Arsenite Mo(V) EPR Signals

parameter[a]	axis 1	axis 2	axis 3	av	angles of noncoincidence (deg)[b] XOX'	YOY'	ZOZ'
			Mercuribenzoate Signal[c]				
g	1.9434	1.9581	1.9687	1.9567			
A(^{199}Hg)	272	285	443	333	5	7	8.6
A(^{201}Hg)	100	105	163	123	5	7	8.6
P(^{201}Hg)	−75	−91	+166		5	7	8.6
A(^{17}O)	34	8.2	4.1	15.4	51	45	27
A(^{33}S)	8.7	7.4	13.8	10.0	nd	nd	nd
			Arsenite Signal[d]				
g	1.9258	1.9718	1.9732	1.9569			
A(^{75}As)	(−)90	(+)128	(−)40	−1	15	0	15
P(^{75}As)	−10	−17	+27		15	0	15

[a] Coupling constants are given in megahertz; 1 mT = 27.4 MHz for $g = 1.9567$. [b] X, Y, and Z refer to the axes (1, 2, 3) in which g is diagonal; X', Y', and Z' refer to the axes in which the coupling is diagonal. nd, not determined. [c] Values given were obtained as described in the text and were used for the simulations of Figures 5–9. Line widths (as half-widths in millitelsa) used along the three axes were as follows in the different simulations: 9-GHz ^{even}Hg, 0.25, 0.24, and 0.25; 9-GHz ^{199}Hg, 0.50, 0.50, and 0.50; 9-GHz ^{201}Hg, 0.37, 0.37, and 0.33; 35-GHz ^{even}Hg and ^{199}Hg, 0.70, 0.60, and 0.70; 35-GHz ^{201}Hg, 0.70, 0.70, and 0.73. Gaussian line shapes were used except for 9-GHz ^{199}Hg, for which Lorenzian line shapes were found to give better fits. Note that if the signs of P(^{201}Hg) are reversed, then an equivalent simulation results; this simulation was only marginally sensitive to the signs of A(^{201}Hg). [d] Data of George & Bray (1983).

Despite this problem, this experiment clearly shows that the interaction with *p*-mercuribenzoate occurs with reduced rather than with oxidized enzyme molecules. Behavior similar to that illustrated for *p*-mercuribenzoate in Figure 4 was found with other mercurials, e.g., *p*-mercuribenzenesulfonate, phenylmercuric ions, and *p*-mercurianiline. Inclusion in the medium of thiols such as β-mercaptoethanol or dithiothreitol (2 mM) did not affect the rate of recovery from inhibition in such experiments.

In considering the inhibition by *p*-mercuribenzoate in greater detail, we note that Figure 2 shows that v_0, the initial velocity as determined by computer fitting, is independent of inhibitor concentration. This provides evidence [cf. Williams et al. (1979)] that, in contrast to inhibition of xanthine oxidase by alloxanthine (Williams & Bray, 1981), no rapid formation of an enzyme–inhibitor complex precedes the slow step in the inhibitory process. On the other hand, v_s decreases rapidly with increasing concentrations of the mercurial (Figure 2). Similarly, k_{obsd} increases linearly with increasing inhibitor concentration (Figure 3), which is also consistent with the slow step being due to slow initial binding of the *p*-mercuribenzoate. It should be noted, particularly, that the point near the vertical axis in Figure 3 was, unlike the other points on the graph, determined from an experiment of the type illustrated in Figure 4 rather than of the type in Figure 1. The fact that the points of Figure 3 lie on a single line is further confirmation of the reversibility of the inhibition process under study.

The complexities of xanthine oxidase turnover, unfortunately, make it difficult to analyze the inhibition fully. In the absence of the inhibitor, the enzyme may turn over by any one of three alternative catalytic cycles. Thus, it may cycle between oxidized enzyme (XO_0) and the two-electron-reduced form (XO_{2e}) or between XO_{2e} and XO_{4e} or, alternatively, between XO_{4e} and XO_{6e} (Olson et al., 1974). Values of k_{cat} and K_m are not known individually with certainty for turnover via any of the three cycles. Thus, the conclusion that *p*-mercuribenzoate inhibits during turnover by binding to a reduced form of the enzyme leaves many questions, as to the species with which it reacts, unanswered. Although, despite these problems, Williams & Bray (1981) attempted to analyze inhibition of xanthine oxidase by alloxanthine, which develops slowly during turnover, we did not follow their treatment, which ignored Michaelis complexes. Instead, we attempted to fit the data to a more complex kinetic model in which two catalytic cycles were included, with the possibility of the inhibitor binding to reduced species occurring in each cycle. Because of its complexity and of the rather arbitrary nature of some of our assumptions, our scheme will not be described in detail. However, the inhibitory constants derived by means of it, from the data in Figures 2 and 3, will nevertheless be quoted, since it is unlikely that the constants would need to be modified greatly if other kinetic models were employed. Thus, the rate constant deduced for reaction of reduced enzyme with *p*-mercuribenzoate at pH 8.2 was about 10^4 M^{-1} s^{-1}, and the K_i value was about 3 μM.

Brumby et al. (1965) reported data, apparently at variance with ours, with inhbition rapidly developed and showing noncompetitive behavior with respect to xanthine, and they interpreted this as indicating that the mercurial reacted at a site not involved in xanthine binding. Such rapid development of inhibition is explained by their having worked at a different pH (9.0) and in a different buffer from the one we employed. Also, in terms of alternative catalytic cycles for xanthine oxidase, noncompetitive inhibition does not necessitate the binding of inhibitory molecules other than at the xanthine site. Binding of the mercurial to reduced forms other than XO_{6e} would be expected to affect both the oxidative half-reaction and the reductive half-reaction. This would cause both slope and intercept effects on double-reciprocal plots and would thus appear as noncompetitive inhibition.

The overall conclusion from our work is that mercurials react relatively slowly and reversibly, in a single step, with reduced xanthine oxidase only to form a complex with a fairly low dissociation constant. Evidence that the site of interaction involves molybdenum is provided by the EPR work described in the following section.

Effect of p-Mercuribenzoate on Mo(V) EPR Signals from Xanthine Oxidase. Figure 5 shows the effect of *p*-mercuribenzoate on active (curves a and b) and desulfo (curves c and d) xanthine oxidase. It can be seen that *p*-mercuribenzoate reacts with active enzyme, under conditions that give close to 100% inhibition, in a manner that causes it to give, in place of the normal Rapid Mo(V) signal (Bray, 1980), a distinct rhombic EPR signal (simulated in Figure 5b′; see Table II for *g* values), which will be referred to as the Mercurial signal. In contrast, only slight changes in the Mo(V) Slow signal from desulfo xanthine oxidase (Bray, 1980) were seen. Changes of greater or of similar magnitude in the Slow signal have been

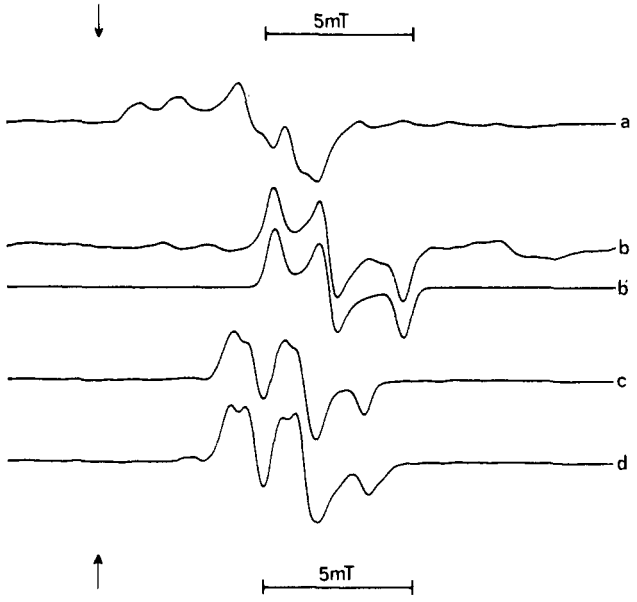

FIGURE 5: Effect of *p*-mercuribenzoate on Mo(V) EPR spectra of active and desulfo xanthine oxidase. All samples were reduced with dithionite in 50 mM Na^+–Bicine, pH 8.2, at 20–25 °C. (a) Active enzyme alone (Rapid signal); (b) active enzyme with *p*-mercuribenzoate (Mercurial signal); (c) desulfo enzyme alone (Slow signal); (d) desulfo enzyme with *p*-mercuribenzoate. (b′) Simple simulation of (b), which allows for $I = 0$ isotopes of mercury only (see Table II for *g* values). Conditions of reduction in (a) were 1 mM dithionite for 1 min; in (b), reduction as in (a) was followed by anaerobic incubation with 1 mM *p*-mercuribenzoate for 2 min. For (c) and (d), reaction conditions were similar to those in (a) and (b), respectively, except that the dithionite concentration was 5 mM, the reduction time was 20 min, and the concentration of mercurial was 5 mM. EPR conditions were 0.1-mT modulation amplitude, 123 K, and 10-mW microwave power. The arrows indicate $g = 2.0037$.

observed in the presence of anions such as nitrate or even with excess of Bicine buffer (Gutteridge et al., 1978b). Therefore the *p*-mercuribenzoate-induced changes in the Slow signal are not thought to indicate chemical modification of the molybdenum site.

The other mercurials studied, namely, phenylmercuric ions, *p*-mercuribenzenesulfonate, *p*-mercuritoluene, and *p*-mercurianiline, also gave Mercurial signals very similar to that obtained with *p*-mercuribenzoate. However, all except *p*-mercuribenzenesulfonate gave also a second quite different EPR signal (not illustrated), which was not investigated in detail.

We carried out limited investigations of conditions affecting intensity of the Mercurial signal, obtained with *p*-mercuribenzoate. It could be generated by brief prereduction of the enzyme with dithionite or a variety of substrates, followed by anaerobic addition of the mercurial. Unlike the Arsenite signal (George & Bray, 1983), the Mercurial signal was not in any modified by the presence of substrate or product molecules (such as purine, xanthine, uric acid, acetaldehyde, or glycolaldehyde) or by inhibitors (such as allopurinol, salicylate, or benzoate).

Kinetic experiments carried out by the rapid freezing method with *p*-mercuribenzoate showed that the Rapid signal declined parallel with the appearance of the Mercurial signal, with this signal developing at a rate that was nearly 10-fold slower than was predicted from the steady-state inhibition studies. However, direct comparison of rate constants is complicated, not only because of the 10^4-fold difference of enzyme concentrations but also because of expected differences in amounts of Mo(V) and Mo(IV) enzyme species in the reduced and turning-over states. The Mercurial signal was found to be unstable to the presence of oxygen, signal intensity being rapidly lost, and activity regained on bubbling oxygen through the solution. Addition of dithionite also caused a reduction in signal intensity, although in this case no activity was regained. This can be attributed to a reduction of the Mo(V) Mercurial signal giving species to a Mo(IV) complex. Maximum intensity of the Mercurial signal determined by integration corresponded to about 30% conversion of molybdenum of the active enzyme to the signal-giving species. Signals due to FADH· and reduced Fe–S centers were readily observable in their normal forms in enzyme samples giving the Mercurial signal. This confirms that only the molybdenum center was affected.

^{199}Hg- and ^{201}Hg-Enrichment Studies. It was noted that the Mercurial signal possessed satellite peaks (see particularly the high-field region of Figure 5b) that appeared too intense to be assigned to naturally abundant ^{97}Mo and ^{95}Mo. It seemed possible that these peaks might arise from hyperfine interaction with the naturally occurring magnetic isotopes of mercury, i.e., ^{201}Hg ($I = {}^3/_2$) and ^{199}Hg ($I = {}^1/_2$), which constitute 13.2% and 16.9%, respectively, of the naturally abundant mercury (other isotopes, referred to below as ^{even}Hg, namely, ^{196}Hg, ^{198}Hg, ^{200}Hg, ^{202}Hg, and ^{204}Hg, make up the balance of 69.9%).

To test this hypothesis, *p*-mercuribenzoate was synthesized as described under Materials and Methods, and Mercurial signals was developed as before. Spectra at 9 GHz from ^{199}Hg- and ^{201}Hg-substituted *p*-mercuribenzoate are shown in curves a and b of Figure 6. It is immediately apparent that the enriched mercury causes large hyperfine splittings of the Mercurial Mo(V) EPR signal, indicating that Mo and Hg are in close proximity in the inhibitory complex. Spectra of such complexity clearly could not be reliably interpreted without using simulations, and to make these more rigorous, we also recorded spectra at 35 GHz, for the Mercurial signal from the different isotopes: natural abundance (Figure 7a); ^{199}Hg (Figure 7b); ^{201}Hg (Figure 7c).

In a recent study of the Arsenite Mo(V) EPR signal from xanthine oxidase (George & Bray, 1983), arsenic was shown to exhibit not only strong anisotropic hyperfine coupling to Mo(V) but also strong quadrupole coupling. ^{201}Hg has a very large nuclear electric quadrupole moment (0.45b). Clearly therefore, the likelihood of quadrupole coupling of ^{201}Hg to Mo(V) has to be considered in interpreting the Mercurial EPR signal. Availability of the mercury isotopes should in principle greatly facilitate rigorous interpretation and simulations of the spectra. Thus, in simulations of the Arsenite signal, since only a single isotope is available, *g* values, hyperfine and quadrupole couplings, and angles all had to be varied together in order to arrive, after much work, at a reasonably satisfactory simulation (George & Bray, 1983). It contrast, for the Mercurial signal it should be possible, successively and unambiguously, to obtain *g* values from the ^{even}Hg features, hyperfine couplings (and angles relating **g** and **A** axes) from ^{199}Hg, and then finally quadrupole couplings from ^{201}Hg. Computer simulations were carried out as described under Materials and Methods. Inclusion of quadrupole coupling was made possible by availability of the programs of Belford and co-workers (Nilges, 1979; Belford & Nilges, 1979; Maurice, 1980).

The ^{199}Hg-enriched Mercurial signal was simulated by using the *g* values from the $I = 0$ part of the unenriched signal (Figure 5b,b′). ^{199}Hg *A* values and angles of noncollinearity (of **A** with **g**) were floated until a good fit (Figures 6a′ and 7b′) was obtained to both 9- and 35-GHz spectra (Figures 6a and 7b) by using the parameters in Table II. It should be

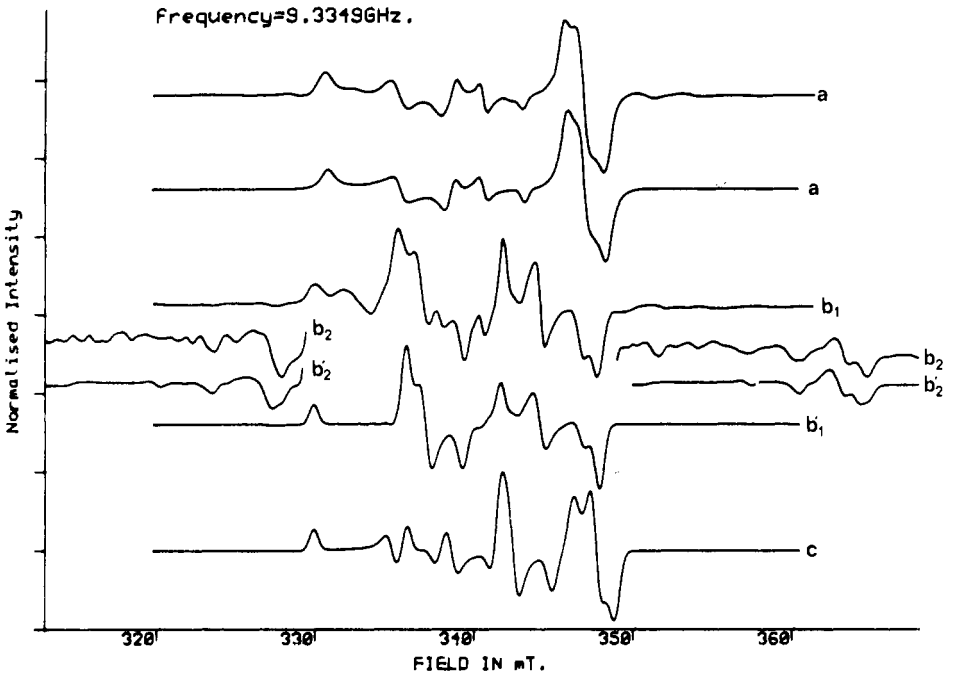

FIGURE 6: Effect of using *p*-mercuribenzoate enriched with ^{199}Hg or ^{201}Hg on appearance of Mercurial signal at 9.3349 GHz. The Mercurial signal was developed and recorded as described in the caption to Figure 5 but by using enriched *p*-mercuribenzoate. (a) Experimental spectrum with ^{199}Hg- (85.3%) enriched *p*-mercuribenzoate. (a′) Simulation of (a) using the parameters in Table II, for ^{199}Hg, and after adding in the simulation of the 14.7% of $I = 0$ (^{even}Hg) isotopes that are present. The spectrum of (b_1) is the signal obtained with ^{201}Hg- (92.0%) enriched *p*-mercuribenzoate. The simulation of this is shown in (b_1') and was based on the parameters for ^{201}Hg of Table II, with an appropriate addition for ^{even}Hg isotopes. High-field and low-field parts of the experimental and simulated ^{201}Hg spectrum are shown at 25-fold higher amplification in (b_2) and (b_2'), respectively. In the case of the experimental spectrum, (b_2), the appropriate amount of the corresponding spectrum for ^{95}Mo-enriched enzyme treated with ^{201}Hg reagent has been subtracted, to simplify the spectrum. (c) Alternative but obviously less good simulation to (b_1'), from which quadrupole coupling has been omitted. [Note that some FADH· signal is present in (b_1).]

noted that although the angles of noncoincidence are all quite small, they are nevertheless determined reasonably precisely from the simulations.

The ^{201}Hg A values were calculated from the ^{199}Hg parameters and the ratio of nuclear g factors ($^{201}g_N/^{199}g_N = -0.371$; Goodman & Raynor, 1970). In agreement with expectations, we found that simulation of the ^{201}Hg spectra excluding quadrupole coupling gave bad fits to the experimental data (see, e.g., Figures 6c and 7d).

The effects on EPR line shapes from quadrupole coupling are due to the electric field gradient at the quadrupole nucleus competing[3] (via the quadrupole coupling) with the external applied magnetic field for allignment of the axis of nuclear spin. When the hyperfine interaction is larger than the quadrupole coupling, then, as discussed by George & Bray (1983) for the Arsenite signal, the main effect is that M_I becomes no longer a good quantum number. This causes a rearrangement of the positions of the allowed ($\Delta M_I = 0$) transitions and an increase in the intensity of the "forbidden" ($\Delta M_I = \pm 1$, ± 2, and ± 3) transitions. On the other hand, if the quadrupole coupling is larger than the hyperfine coupling, then (at most orientations) the forbidden transitions with $\Delta M_I = \pm 2$ come to dominate the spectrum (Muha, 1978), the relative intensities of the $\Delta M_I = 0$, $\Delta M_I = \pm 1$, and $\Delta M_I = \pm 3$ transitions being much smaller.

Inclusion of large quadrupole coupling improved the fit of the ^{201}Hg simulation greatly (Figures 6b$_1$′ and 7c′). It was found, however, that at the level of quadrupole coupling that had to be included, the main features of the simulated spectrum were quite insensitive to the precise coupling that was assumed. Examination of the various components of the simulation (Figure 8) confirmed that the features of largest amplitude were due to $\Delta M_I = \pm 2$ transitions. The positions of these features were found [as expected; cf. Muha (1978)] not to vary significantly on increasing P_3 (the largest axis of P), after P_3 was made greater than about 60 MHz. Therefore, in order precisely to evaluate the quadrupole coupling, we turned our attention to the weak satellites in the spectrum, due to $\Delta M_I = 0$ and $\Delta M_I = \pm 1$ transitions (Figure 8b,c). To identify these lines in the experimental spectrum, we had to eliminate possible confusion with features due to naturally abundant ^{95}Mo and ^{97}Mo (these have $I = {}^5/_2$ and similar g_N). We achieved this (Figure 6b$_2$) by preparing a doubly enriched sample (^{95}Mo and ^{201}Hg) and subtracting its spectrum (not shown), in the appropriate proportion, from the original spectrum. The final simulations (Figures 6b$_1$′,b$_2$′ and 7c′) agree well with the experimental spectra in all features, including these satellite lines (Figure 6b$_2$). All the parameters of the Mercurial signal, as used in the simulations, are summarized in Table II. It should be noted that the best fit was found to be achieved when **A** and **P** were held collinear. The high quality of all the simulations that we have obtained, by using a single set of parameters, for spectra recorded for the various isotopes at both 9 and 35 GHz gives us considerable confidence in the uniqueness of our interpretations and in the accuracy of the parameters.

A notable feature of the Mercurial signal is that the line widths are very much larger in the ^{199}Hg signal than in the ^{even}Hg signal. This is particularly apparent in Figure 6a, where the three small central features of the spectrum are due to ^{even}Hg, while the three obviously broader corresponding features at low field are due to ^{199}Hg. This broadening cannot be due to a second weakly coupled Hg since if this were the case, then the central lines also would be broadened in the enriched sample. Line widths employed in the simulations are

[3] Just as an electric field will exert a torque on an electric dipole, so an electric field gradient will exert a torque on an electric quadrupole.

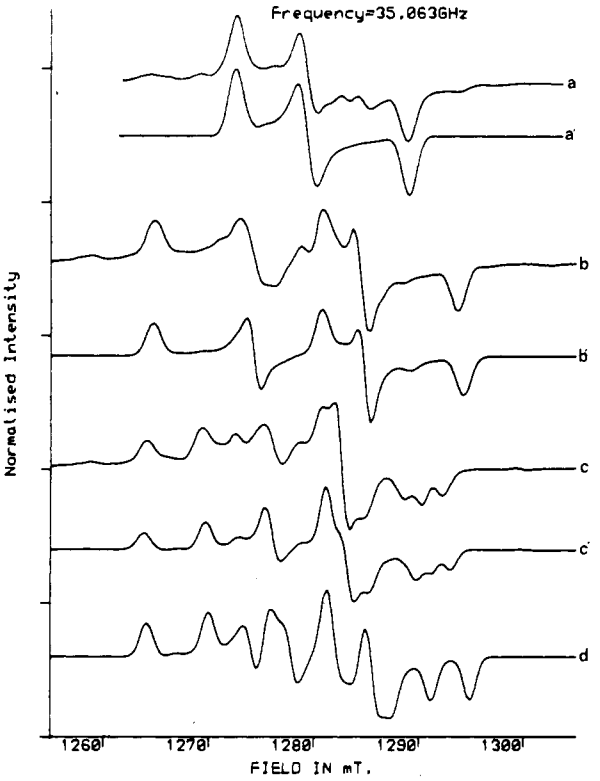

FIGURE 7: Effect of using *p*-mercuribenzoate, unenriched or enriched with ^{199}Hg or ^{201}Hg, on appearance of Mercurial signal at 35.063 GHz. The signal was developed as described in the caption to Figure 5, by using (a) the natural abundance of mercury isotopes, (b) ^{199}Hg (85.3% enriched), or (c) ^{201}Hg (92.0% enriched). The corresponding simulations are shown in (a′), (b′), and (c′), respectively, on the basis of the parameters of Table II; appropriate additions have been made to (b′) and (c′) for ^{even}Hg isotopes. (d) Simulation of (c′) but with quadrupole coupling omitted. EPR conditions were 123 K, 10-dB microwave power attenuation, and 0.5-mT modulation amplitude.

listed in Table II (footnote *c*); widths were found to change little with temperature down to 5.3 K. To obtain further information, we investigated the saturation behavior of the signal. Careful measurements were made and data fitted to (Beinert & Orme-Johnson, 1967)

$$S \propto [P/(1 + P/P_{1/2})^b]^{1/2} \quad (2)$$

where S is signal intensity, P is incident microwave power, $P_{1/2}$ is the power for half-saturation, and b is a constant. Small differences, only, between saturation behavior of the ^{even}Hg and the ^{199}Hg Mercurial signals were found, with the inhomogeneity parameter, b, diminished by about 10% for ^{199}Hg. It therefore seems clear, that the observed broadending of the lines for this isotope cannot be due primarily to any extra method of relaxation, invoked by the large ^{199}Hg hyperfine coupling. The most probable reason for the larger width seems to be the presence of strain coupling to the hyperfine interaction [i.e., so-called K strain; cf. Hagen (1981)]. This phenomenon is due to different molecules in the frozen solution possessing very slightly different **A** tensors and thus should be essentially frequency independent. In agreement with this hypothesis, it can be seen (Table II, footnote *c*) that at 35 GHz the ^{199}Hg Mercurial signal line widths are similar to those of the ^{even}Hg signal (at 35 GHz increased line widths would be expected to "hide" any broadening from K strain). In addition, some broadening should also be seen in the ^{201}Hg signal (at 9 GHz), and in agreement with this, some features of Figure 6b do seem to be broadened.

Substitution with ^2H, ^{17}O, or ^{33}S. Much information has been obtained on the structures of Mo(V) EPR signal giving enzyme species from substitution studies employing ^2H, ^{17}O, and ^{33}S (Bray, 1980; Malthouse et al., 1981; Bray & Gutteridge, 1982). We therefore carried out studies on the Mercurial signal with these isotopes, comparable to those reported for the Arsenite signal by George & Bray (1983).

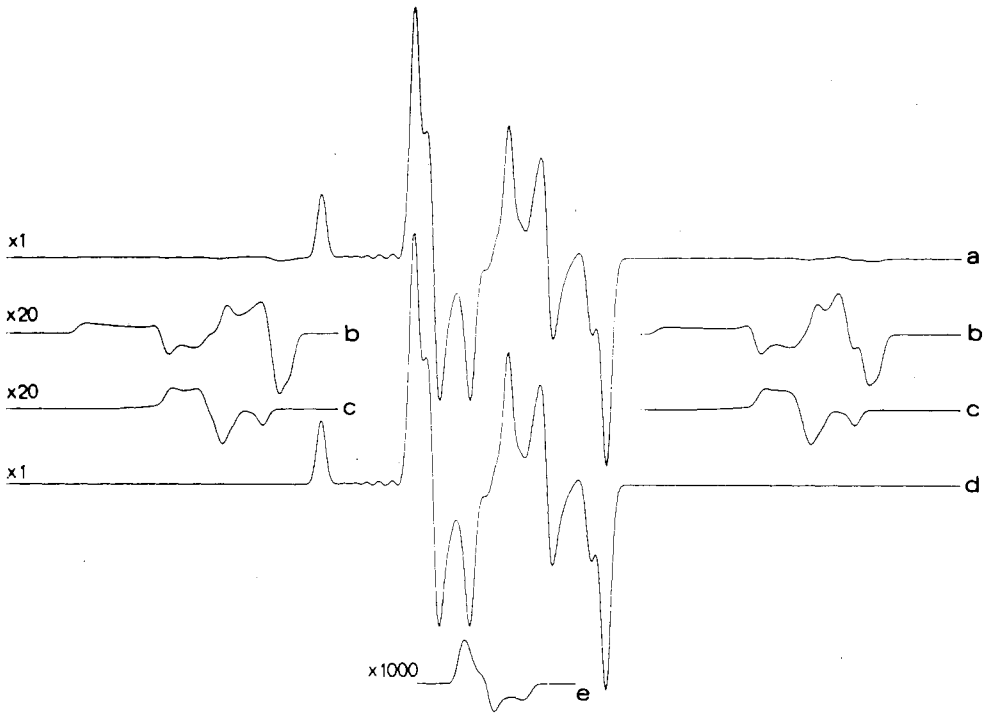

FIGURE 8: Contribution of different transitions to simulated ^{201}Hg Mercurial signal at 9.3349 GHz. (a) Complete simulation for 100%-enriched ^{201}Hg Mercurial signal, on the basis of the parameters of Table II; (b–e) different components that, added together, give (a). Thus, (b)–(e), respectively, correspond at the different amplifications indicated to the following transitions: $\Delta M_I = 0$; $\Delta M_I = \pm 1$; $\Delta M_I = \pm 2$; $\Delta M_I = \pm 3$. Note that (b) and (c) have no features in the central region of the spectrum and that the small oscillations to the low-field side of the main "upward" feature in (a) and (d) are computing artifacts. It is clear that the main features of the ^{201}Hg spectrum are due to the $\Delta M_I = \pm 2$ transitions.

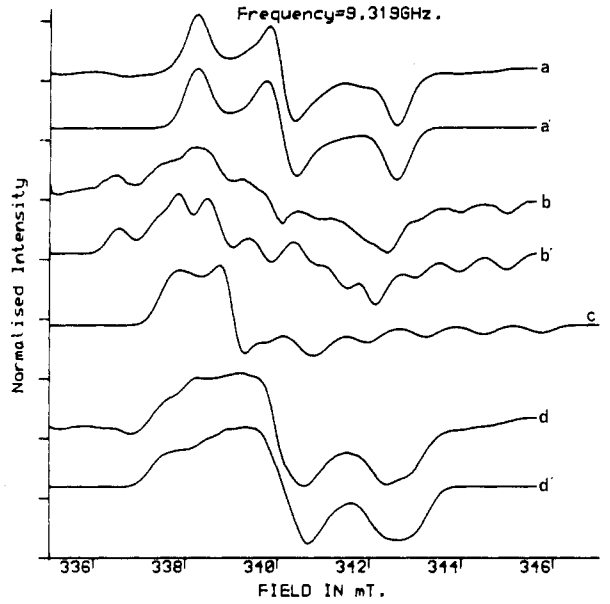

FIGURE 9: Effect of substitution with ^{17}O or with ^{33}S on ^{even}Hg region of Mercurial signal at 9.319 GHz. Samples giving the Mercurial signal were prepared by using unenriched *p*-mercuribenzoate as described in the caption to Figure 5. Enrichment with ^{17}O or ^{33}S was achieved as described under Materials and Methods. (a) Control sample without enrichment; (a′) simulation of (a) including only $I = 0$ isotopes. (b) Difference spectrum (corresponding to 100% ^{17}O) from an ^{17}O (52%-enriched) Mercurial signal [obtained by subtracting 48% of (a) from the original experimental spectrum]. (b′) Simulation of (b) using the parameters given in Table II. (c) Obviously unsatisfactory simulation of (b), where *g* and *A* were held collinear, all other parameters being as in (b′). The effect of using ^{33}S-enriched xanthine oxidase is shown in (d). This spectrum was obtained by difference from an experimental ^{33}S (59%-enriched) sample, by subtracting 41% of (a); (d) 100% ^{33}S. (d′) Simulation of (d) using the parameters in Table II.

Developing the Mercurial signal in ^2H_2O in place of ordinary water had no effect on the signal, showing the absence of exchangeable protons detectably coupled to Mo(V) in the signal-giving species. The Mercurial signal from ^{17}O-enriched xanthine oxidase is shown in Figure 9b. Good simulations of this (Figure 9b′) were obtained when strong anisotropic hyperfine coupling from one oxygen, with highly noncollinear **g** and **A** (Table II), was assumed. Figure 9c shows the markedly inferior simulation obtained by assuming the axes to be collinear.

The effect of using ^{33}S-substituted xanthine oxidase on the Mercurial signal is shown in Figure 9d with the simulation in Figure 9d′. For this spectrum, since the splitting is small, the resolution of the hyperfine lines was not sufficient to determine if **g** and **A** were noncollinear. Their axes were therefore held collinear in all simulations, although this is probably not the case in reality. The hyperfine coupling was again found to be anisotropic, although less so than for ^{17}O.

Structure of Mercurial Signal Giving Species. The structure we propose as the signal-giving species for the Mercurial signal is illustrated in Chart IA. The preferred structure of George & Bray (1983) for the Arsenite species is shown, for comparison, in Chart IB. Evidence for the structure comes from both biochemical and spectroscopic data. As already stated, the latter clearly shows that mercury is close to molybdenum. From the former, it is clear that only the active enzyme, and not the desulfo enzyme, reacts with mercurials. This must make the cyanide-labile sulfur of the active enzyme, lost on conversion to the desulfo enzyme, the likely site of mercurial interaction. The EPR evidence (Gutteridge et al., 1978b; Bray & Gutteridge, 1982) is that this sulfur is present

Chart I: Proposed Structures of (A) the Mercurial and (B) the Arsenite Mo(V) EPR Signal Giving Species[a]

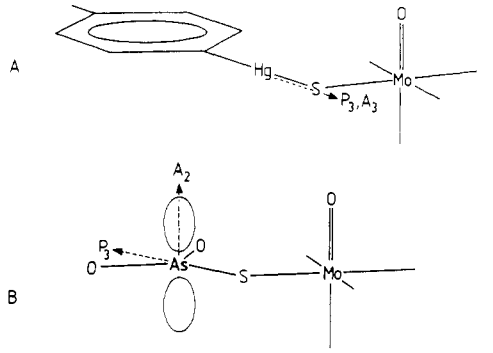

[a] The structure of the Arsenite species is the one preferred by George & Bray (1983).

as MoSH in the reduced but not in the oxidized enzyme, and this evidence is supported to some extent by EXAFS (Cramer et al., 1981). If this evidence is accepted, then the Mo–S–Hg structure proposed in Chart IA becomes unambiguous, when it is remembered, first, that –SH groups are the usual reaction site for mercurials with proteins [cf. Madsen (1963)] and, second, that xanthine oxidase reacts with them only when it is in a reduced state. More detailed consideration of the EPR parameters supports and amplifies these conclusions.

As previously stated, the ^{201}Hg quadrupole coupling is directly indicative of the size of the electric field gradient at the mercury. For a linear arrangement of atoms around mercury (as would be expected), the largest principal axis of the electric field gradient tensor, and thus the largest axis of **P**, should be directed along the linear sp bond system of the mercury (Kerr et al., 1976; Gordy et al., 1966). Reports of ^{201}Hg quadrupole coupling are scarce in the literature, and the only well-investigated systems are mercuric chloride [by NQR; cf. Patterson et al. (1973)] and the $\cdot CH_2HgCl$ radical (by EPR; Kerr et al., 1976). For the latter system, the quadrupole coupling[4] to ^{201}Hg (900 MHz) can be seen to be very similar to that of the Mercurial signal (960 MHz). This close similarity provides some support for the proposed structure (Chart IA), as an Hg–S bond, like an Hg–Cl bond, would be expected to have significant ionic character.

The largest principal axis of **A** was found to be collinear with the largest axis of **P** (Table II). If the proposal that the largest axis of **P** runs along a linear S–Hg–C bond is correct, then the hyperfine coupling would be most probably due to spin density in this bond.

The hyperfine coupling to ^{33}S (Table II) is much smaller than that to mercury, even after appropriate allowance has been made (Goodman & Raynor, 1970) for the limiting values of such couplings. Similar low coupling to ^{33}S has been observed for the Arsenite signal (George & Bray, 1983), which was considered to have a similar structure (Chart I). As discussed by these workers, this low ^{33}S coupling is not inconsistent with the proposed structures as, in d^1 systems, ligands adjacent to the metal ion (i.e., ^{33}S) tend to be weakly coupled as they lie on the nodes of the ground-state orbital. The atoms adjacent to these ligands (i.e., Hg or As), however, are often more strongly coupled. Although the exact mechanism of coupling is obscure, this would be related to the nonlinearity of the Mo–S–Hg system holding the mercury into a region of higher electron density. Alternatively, an analogy

[4] Where quadrupole coupling constants (e^2qQ) are quoted, these are related to the largest axis of **P** (P_3) by $e^2qQ = 2I(2I-1)P_3 = 6P_3$ (for $I = {}^3/_2$).

might be suggested with the coupling of β-protons in free-radical systems (Barefield, 1970) where hyperconjugation is responsible for a large β-proton coupling (while the α-carbon coupling remains small).

An alternative structure for the Mercurial signal-giving species might be suggested in which the mercury is bound directly to molybdenum [compounds with Mo–Hg bonds are well-known; see Cotton & Wilkinson (1980)]. However, this seems to be excluded both by the lack of reaction of desulfo enzyme with mercurials and by the size of the ^{201}Hg quadrupole coupling (since close proximity of an atom such as molybdenum would cause the ^{201}Hg quadrupole coupling to be much larger than in $\cdot CH_2HgCl$).

The hyperfine coupling to oxygen (Table II) is highly anisotropic, which indicates a large p-orbital contribution in its bonding to molybdenum, which would be expected for a terminally bound oxygen (the magnitude of the coupling is in the range expected for ligation of oxygen to molybdenum). It is shown (Chart IA) in an axial position even though the ^{17}O hyperfine coupling is larger than expected from EPR studies of a model compound (Hanson et al., 1981). Such a group would be expected to cause the ground-state 4d orbital to be in the plane perpendicular to the Mo–O bond. It is conceivable, however, that there is another oxygen ligand, undetected because of the small size of its hyperfine coupling or because of its lack of exchangeability, that occupies this position and that the strongly coupled oxygen that is detected actually lies in the equatorial plane.

Comparison of Mercurial and Arsenite Signal Giving Species. The proposed structure of the Mercurial signal giving species is similar to that for the Arsenite signal (George & Bray, 1983); these are shown in Chart I. Although the relative orientations of the largest axes of **A** and **P** differ [see George & Bray (1983) for a discussion of this in the Arsenite signal], values of the hyperfine couplings to As and Hg (Table II) (after allowing for the limiting values of these) are similar. This presumably indicates similar spin densities on these atoms in the signal-giving species. As was found for the Arsenite signal, **g** for the Mercurial signal (although in this case considerably less anisotropic, Table II) has lower principal values than are usually excountered in Mo(V) signals from molybdo enzymes (Bray, 1980). Such low *g* values are probably due to spin–orbit coupling involving mercury (or arsenic for the Arsenite signal).

The stability and kinetics of formation of the arsenite and *p*-mercuribenzoate complexes differ markedly. *p*-Mercuribenzoate was found to react only with reduced enzyme and reacted more readily than did arsenite. On the other hand, the arsenite complex can be formed also, though only slowly, from the oxidized enzyme. Also, once formed, the arsenite complex is fully stable to oxidation and reduction of the enzyme, whereas the mercurial complex is decomposed on reoxidizing the enzyme. The origin of these differences is uncertain.

Acknowledgments

We are greatly indebted to Dr. R. L. Belford for making his EPR simulation program available to us, and we thank Teresa Wilkinson for technical assistance.

Registry No. *p*-Hg^+–C_6H_4–COO^-, 87101-04-0; *p*-Hg^+–C_6H_4–SO_3^-, 87101-05-1; *p*-Hg^+–C_6H_4–NH_3^+, 87101-06-2; *p*-Hg^+–C_6H_4–CH_3, 36484-64-7; *p*-Hg^+–C_6H_5, 23172-37-4; Mo, 7439-98-7; xanthine oxidase, 9002-17-9.

References

Barber, M. J., & Siegel, M. L. (1983) *Biochemistry 22*, 618–624.

Barefield, M. (1970) *J. Chem. Phys. 53*, 3835–3843.

Beinert, H., & Orme-Johnson, W. H. (1967) in *Magnetic Resonance in Biological Systems* (Ehrenberg, A., Malmström, B., & Vänngård, T., Eds.) pp 221–247, Pergamon, Oxford.

Belford, R. L., & Nilges, M. J. (1979) Symposium on Electron Paramagnetic Resonance Spectroscopy, Rocky Mountain Conference on Analytical Chemistry, Denver, CO, Aug 1979 (in press).

Bray, R. C. (1975) *Enzymes, 3rd Ed. 12*, 299–419.

Bray, R. C. (1980) *Adv. Enzymol. Relat. Areas Mol. Biol. 51*, 107–165.

Bray, R. C. (1982) in *Flavins and Flavoproteins* (Massey, V., & Williams, C. H., Eds.) pp 775–785, Elsevier, Amsterdam.

Bray, R. C., & Gutteridge, S. (1982) *Biochemistry 21*, 5992–5999.

Bray, R. C., Barber, M. J., & Lowe, D. J. (1978) *Biochem. J. 171*, 653–658.

Brumby, P. E., Miller, R. W., & Massey, V. (1965) *J. Biol. Chem. 240*, 2222–2227.

Cha, S. (1975) *Biochem. Pharmacol. 24*, 2177–2185.

Cha, S. (1976) *Biochem. Pharmacol. 25*, 2695–2702.

Cotton, F. A., & Wilkinson, G. (1980) in *Advanced Inorganic Chemistry*, 4th ed., Wiley, New York.

Cramer, S. P., Wahl, R., & Rajagopalan, K. V. (1981) *J. Am. Chem. Soc. 103*, 7721–7727.

Fridovich, I., & Handler, P. (1958) *J. Biol. Chem. 231*, 899–911.

George, G. N. (1983) Ph.D. Thesis, University of Sussex.

George, G. N., & Bray, R. C. (1983) *Biochemistry 22*, 1013–1021.

Goodman, B. A., & Raynor, J. B. (1970) *Adv. Inorg. Chem. Radiochem. 13*, 135–362.

Gordy, W., Smith, W. V., & Trambarulo, R. F. (1966) *Microwave Spectroscopy*, p 267, Dover, New York.

Gutteridge, S., Tanner, S. J., & Bray, R. C. (1978a) *Biochem. J. 175*, 869–878.

Gutteridge, S., Tanner, S. J., & Bray, R. C. (1978b) *Biochem. J. 175*, 887–897.

Hagen, W. R. (1981) *J. Magn. Reson. 44*, 447–469.

Hanson, G. R., Brunette, A. A., McDonnell, A. C., Murray, K. S., & Wedd, A. G. (1981) *J. Am. Chem. Soc. 103*, 1953–1959.

Harris, J., & Hellerman, L. (1956) in *Inorganic Nitrogen Metabolism* (McElroy, W. D., & Glass, B., Eds.) pp 565–570, John Hopkins Press, Baltimore, MD.

Hart, L. I., McGartoll, M. A., Chapman, H. R., & Bray, R. C. (1970) *Biochem. J. 116*, 851–864.

Hille, R., Stewart, R. C., Fee, J. A., & Massey, V. (1983) *J. Biol. Chem. 258*, 4849–4856.

Kerr, C. M., Wargon, J. A., & Williams, F. (1976) *J. Chem. Soc., Faraday Trans. 2 72*, 552–556.

Lowe, D. J. (1978) *Biochem. J. 171*, 649–651.

Madsen, N. B. (1963) in *Metabolic Inhibitors* (Hochster, R. N., & Quastel, J. H., Eds.) Vol. II, Chapter 21, Academic Press, New York.

Malthouse, J. P. G., George, G. N., Lowe, D. J., & Bray, R. C. (1981) *Biochem. J. 199*, 626–637.

Massey, V., & Edmondson, D. (1970) *J. Biol. Chem. 245*, 6595–6598.

Massey, V., Brumby, P. E., Palmer, G., & Komai, H. (1969) *J. Biol. Chem. 244*, 1682–1691.

Maurice, A. M. (1980) Ph.D. Thesis, University of Illinois.

Muha, G. M. (1978) *J. Magn. Reson. 32*, 121–129.
Nilges, M. J. (1979) Ph.D. Thesis, University of Illinois.
Nishino, T., Tsushima, K., Hille, R., & Massey, V. (1982) *J. Biol. Chem. 257*, 7348–7353.
Olson, J. S., Ballou, D. P., Palmer, G., & Massey, V. (1974) *J. Biol. Chem. 249*, 4362–4382.
Patterson, D. B., Peterson, G. E., & Carnevale, A. (1973) *Inorg. Chem. 12*, 1282–1286.
Pick, F. M., McGartoll, M. A., & Bray, R. C. (1971) *Eur. J. Biochem. 18*, 65.
Whitmore, F. C., & Woodward, G. E. (1941) *Organic Syntheses*, Collect. Vol. I, p 159, Wiley, New York.
Williams, J. W., & Bray, R. C. (1981) *Biochem. J. 195*, 753–760.
Williams, J. W., Morrison, J. F., & Duggleby, R. G. (1979) *Biochemistry 18*, 2567–2573.

Rapid Kinetics of Agonist Binding and Permeability Response Analyzed in Parallel on Acetylcholine Receptor Rich Membranes from *Torpedo marmorata*†

Thierry Heidmann, Julius Bernhardt, Eberhard Neumann, and Jean-Pierre Changeux*

ABSTRACT: Excitable acetylcholine receptor rich membrane fragments from *Torpedo marmorata* have been used to measure, *in parallel*, (1) the permeability response to the fluorescent cholinergic agonist Dns-C_6-Cho (in the 0.1 μM to millimolar concentration range) characterized by both the initial rate of Li^+ transport and the rate of channel closure using the rapid-mixing quench-flow technique and (2) the kinetics of interaction of Dns-C_6-Cho with the acetylcholine receptor sites using the rapid-mixing stopped-flow technique. Analysis of the kinetics of Dns-C_6-Cho *binding* in the millisecond to minute time scale leads to the identification of *at least* three conformational states of the acetylcholine receptor: a "low-affinity" one ($\sim$50 μM) that can be interconverted in the fraction of a second to a transient state of "intermediate affinity" ($\sim$1 μM), followed by the final stabilization, in the second to minute time range, of a state of "high affinity" ($\sim$3 nM). Comparison of Dns-C_6-Cho binding data with the permeability response to the same agonist demonstrates that the binding to the low-affinity conformation(s) of the acetylcholine receptor sites coincides with the triggering of the permeability increase—or "activation"—and the transitions to the intermediate- and high-affinity states with the two-step process of channel closing—or "desensitization". The data are interpreted in terms of a minimum four-state "allosteric" model for the acetylcholine receptor.

At the neuromuscular junction and at the electromotor synapse, the neurotransmitter acetylcholine (AcCh)[1] elicits two distinct classes of reactions. Applied as a brief (millisecond) pulse of high concentration (fraction of millimolar), AcCh causes the rapid opening—or "activation"—of transmembrane ion channels selective for cations (Katz, 1966). When maintained for a longer period of time (fraction of a second or minutes), in contact with the postsynaptic membrane, and at a sufficient concentration (approximately micromolar), AcCh initiates a complex time-dependent decrease of the permeability response—or "desensitization". Both classes of reactions have been kinetically analyzed by various electrophysiological techniques [reviews in Adams (1981), Feltz & Trautmann (1982), and Neher et al. (1983)]. The opening of the ion channel by AcCh takes place in the fraction of millisecond to millisecond time scale and in an "all-or-none" manner at the molecular level (Katz & Miledi, 1970; Neher & Sakmann, 1976). On the other hand, the desensitization reaction can be decomposed in, at least, two steps: a rapid one in the 100 ms to second time scale and a slow one in the range of seconds (Sakmann et al., 1980; Feltz & Trautmann, 1982).

Current biochemical investigations have led to the unambiguous identification of the protein that binds the neurotransmitter, the *AcCh-receptor* (AcChR) sensu stricto, and its purification in milligram quantities has been achieved by starting with postsynaptic membrane fragments isolated from fish electric organs. Its functional reincorporation into artificial membranes or liposomes has further demonstrated that this single protein still mediates AcCh-regulated ion translocation and thus comprises the associated ion channel [reviews in Changeux (1981), Popot (1983), and Anholt et al. (1983)]. The elementary AcChR "light form" is a heterologous pentameric protein made up of four distinct and strongly associated polypeptide chains $\alpha_2\beta\gamma\delta$ [reviews in Karlin (1980), Changeux (1981), and Conti-Tronconi & Raftery (1982)]. Covalent (and noncovalent) analogues of AcCh and snake venom α toxins selectively label the α chains, which therefore carry at least part of the AcCh binding sites (two sites per receptor molecule) [references cited in Tzartos & Changeux (1983)]. Potential markers of the ion channel such as the

† From the Neurobiologie Moléculaire and Laboratoire Associé au Centre National de la Recherche Scientifique, Interactions Moléculaires, Institut Pasteur, 75724 Paris Cedex 15, France (T.H., J.B., and J.-P.C.), and the Max-Planck-Institut für Biochemie, 8033-Martinsried bei, Munchen, FRG (J.B. and E.N.). *Received April 7, 1983.* This work was supported by grants from the Muscular Dystrophy Association of America, the Fondation de France, the Collège de France, the Ministère de la Recherche et de l'Industrie, the Centre National de la Recherche Scientifique, the Institut National de la Santé et de la Recherche Médicale, and the Commissariat à l'Energie Atomique. We gratefully acknowledge an EMBO short-term stipend (to J.B.) and the support of the Deutsche Forschungsgemeinschaft (Grant 227 to E.N.).

[1] Abbreviations: AcCh, acetylcholine; AcChR, acetylcholine receptor; Dns-C_6-Cho, 6-[5-(dimethylamino)-1-naphthalenesulfonamido]hexanoic acid β-(methobromide) ethyl ester.

0006-2960/83/0422-5452$01.50/0